

# Near-infrared imaging and the $K - z$ relation for radio galaxies in the 7C Redshift Survey

Chris J. Willott<sup>1,2\*</sup>, Steve Rawlings<sup>2</sup>, Matt J. Jarvis<sup>3</sup>, Katherine M. Blundell<sup>2</sup>

<sup>1</sup>*Herzberg Institute of Astrophysics, National Research Council, 5071 West Saanich Rd, Victoria, B.C. V9E 2E7, Canada*

<sup>2</sup>*Astrophysics, Department of Physics, Keble Road, Oxford, OX1 3RH, U.K.*

<sup>3</sup>*Sterrewacht Leiden, Postbus 9513, 2300 RA Leiden, the Netherlands*

5 November 2018

## ABSTRACT

We present  $K$ -band imaging of all 49 radio galaxies in the 7C–I and 7C–II regions of the 7C Redshift Survey (7CRS). The low-frequency (151 MHz) selected 7CRS sample contains all sources with flux-densities  $S_{151} > 0.5$  Jy in three regions of the sky. We combine the  $K$ -band magnitudes of the 7CRS radio galaxies with those from the 3CRR, 6CE and 6C\* samples to investigate the nature of the relationship between  $K$ -magnitude and redshift and whether there is any dependence upon radio luminosity. We find that radio galaxies appear to belong to a homogeneous population which formed the bulk of their stars at high redshifts ( $z_f > 5$ ) and evolved passively from then until they reach a mean present-day luminosity of  $3 L_*$ . We find a significant difference between the  $K$ -magnitudes of the 7CRS and 3CRR radio galaxies with the 7CRS galaxies being  $\approx 0.55$  mag fainter at all redshifts. The cause of this weak correlation between stellar and radio luminosities probably lies in mutual correlations of these properties with the central black hole mass. We compare the evolution-corrected host luminosities at a constant radio luminosity and find that the typical host luminosity (mass) increases by approximately  $1 L_*$  from  $z \sim 2$  to  $z \sim 0.5$  which, although a much smaller factor than predicted by semi-analytic models of galaxy formation, is in line with results on optically-selected quasars. Our study has therefore revealed that the small dispersion in stellar luminosity of radio galaxies around  $3 L_*$  includes subtle but significant differences between the host galaxies of extreme- and moderate-power radio sources at fixed redshift, and between those of high- and low-redshift radio sources at fixed radio luminosity.

**Key words:** galaxies: evolution – galaxies: formation – galaxies: active – radio continuum: galaxies

## 1 INTRODUCTION

The luminous radio and narrow-line emission from radio galaxies provides a convenient method for selecting at least a subset of the most massive galaxies at a wide range of redshifts. At low redshifts, powerful radio sources are known to be triggered only within massive elliptical galaxies (Bettoni et al. 2001). The near-infrared magnitudes of radio galaxies out to beyond  $z = 5$  (De Breuck et al. 2002) suggest that radio galaxies at all redshifts have extreme stellar masses. Standard CDM-based galaxy formation models predict that structures grow in a hierarchical fashion. The formation

epoch and evolution of the most massive galaxies is therefore of relevance to such models.

The near-infrared  $K$ -band emission from radio galaxies is dominated by stellar light in most cases (Best, Longair & Röttgering 1998; Simpson, Rawlings & Lacy 1999). Although narrow emission lines can dominate in some objects (Eales & Rawlings 1993), this is confined to only the most radio-luminous objects at  $z > 2$  (e.g. Jarvis et al. 2001a). The  $K$ -band magnitudes of radio galaxies from the bright 3CRR sample (Laing, Riley & Longair 1983) follow a tight correlation with redshift (Lilly & Longair 1984). The nature of this ‘ $K - z$  relation’ showed that the stellar luminosities of high redshift radio galaxies are considerably more luminous than the curve representing no stellar evolution and consistent with a passively evolving population which formed at

\* Email: chris.willott@nrc.ca

high redshifts. The small dispersion in  $K$ -magnitudes at a given redshift evident in the 3CRR sample is also found in other complete samples and continues up to at least  $z = 3$  (Jarvis et al. 2001a). Together these facts suggest that radio galaxies are a homogeneous population which formed the bulk of their stars at high-redshifts ( $z_f > 5$ ) and evolved passively from then until the present day.

Eales et al. (1997) presented  $K$ -band data for radio galaxies in the 6CE sample which has a flux-density limit a factor of about 5 times lower than the 3CRR sample. They found that the less radio-luminous 6CE galaxies tended to have fainter  $K$ -band magnitudes than 3CRR galaxies at similar redshifts. They determined a difference of 0.6 mag for the two samples at  $z > 0.6$ , but found that at  $z < 0.6$  there was no difference between the samples. Such an evolutionary change in the radio-luminosity dependence of stellar luminosities was interpreted by Best et al. (1998) as due to radio luminosity being more closely related to the mass of the black hole at high redshifts than at low redshifts where availability of fuel would dominate. Lacy, Bunker & Ridgway (2000) used near-infrared imaging of sources from the 7C-III region of the 7C Redshift Survey (7CRS; selected at a flux-density limit a factor of 20 times lower than 3CRR) to show that radio galaxies at  $0.8 < z < 1.4$  from both the 7CRS and 6CE samples are fainter by 0.4 mag than 3CRR galaxies. They suggest two possible reasons for this correlation between host and radio luminosities: (i) AGN-related contamination of the stellar light; (ii) a correlation of both luminosities with the mass of the central black hole.

It is important in studies of the properties of radio galaxies that the samples used should be close to complete in terms of secure optical identifications and redshifts. There are several biases which can appear for incomplete samples, such as missing objects with the weakest emission lines because spectra are harder to obtain. Similarly, spectroscopically targeting the faintest sources at  $K$ -band (e.g. with the aim of finding the highest redshift galaxies, De Breuck et al. 2001) will bias the sample in terms of its  $K - z$  relation.

In this paper we present near-infrared imaging of a completely-identified sample of radio sources selected at 151 MHz from the 7C catalogue. This sample (regions 7C-I and 7C-II of the 7CRS) has 90% spectroscopic redshift completeness (Willott et al. 2002) with reasonable estimates of the redshifts for the remaining few sources from multi-colour photometry (Willott, Rawlings & Blundell 2001). We combine these data with those from the 3CRR, 6CE (Rawlings et al. 2001), 6C\* (Jarvis et al. 2001a,b) and 7C-III (Lacy et al. 2000) samples to define the  $K - z$  relation from over 200 radio galaxies in samples with high spectroscopic completeness.

In Section 2 we present the  $K$ -band imaging observations for all the radio galaxies in 7C-I and 7C-II. In Section 3 we discuss corrections made to the observed  $K$ -magnitudes from all the samples to produce a uniform dataset and then discuss the form of the  $K - z$  relation and its evolutionary interpretation. Section 4 investigates evidence for a correlation between the stellar luminosity (mass) of the host galaxy and the radio luminosity and also considers the evolution in stellar luminosity at a fixed radio luminosity. The conclusions are given in Section 5. In the Appendix we present  $K$ -band images as finding charts for the 7C-I and 7C-II quasars and broad-lined radio galaxies whose properties were dis-

cussed in Willott et al. (1998). We assume throughout that  $H_0 = 70 \text{ km s}^{-1} \text{ Mpc}^{-1}$ ,  $\Omega_M = 0.3$  and  $\Omega_\Lambda = 0.7$ .

## 2 NEAR-INFRARED IMAGING

### 2.1 Observations

All members of the 7C Redshift Survey (except the flat-spectrum quasar 5C7.230 and 3C200) have been imaged at  $K$ -band to provide an identification for spectroscopy, to determine the near-IR morphology and magnitude. These observations were made over several observing runs at the United Kingdom Infrared Telescope (UKIRT) on Mauna Kea, Hawaii. Sky conditions were photometric on all nights. These observations used the IRCAM3 near-infrared detector. IRCAM3 is a SBRC InSb  $256^2$  array with a pixel scale of  $0.286 \text{ arcsec pix}^{-1}$  and field of view of  $73 \times 73 \text{ arcsec}^2$ .

In order to subtract the rapidly changing sky background, provide a good flat-field and avoid problems due to cosmic rays and bad pixels, the observing strategy used was to offset the position of the telescope by 10 arcsec between each 60 second exposure. The offsets were arranged in a  $3 \times 3$  mosaic. Most sources were observed for one of these mosaics (total exposure time 9 minutes) or a multiple thereof. For some of the brightest sources less than 9 minutes was required to achieve good signal-to-noise. In a few cases, individual 60 second frames were corrupted by the electronics or poor guiding problems and these were discarded. The observing log for  $K$ -band observations of the 7C radio galaxies is given in Table 1. The observations of quasars and broad-lined radio galaxies in the sample were described in Willott et al. (1998), but the images are presented in the Appendix of this paper.

### 2.2 Data reduction

Data reduction was performed using the IRAF package. Dark frames of equal integration time to the science frames were taken on all nights. An average dark frame was subtracted from each of the images taken. A flat-field was created for each field observed by combining all of the data frames from the field using a median filter. All the dark-subtracted frames were divided by the normalized flat-field. Registering of the offset frames was performed using the brightest stars in the images. To correct for the small effects of atmospheric extinction at  $K$ -band, each individual frame was scaled by a factor of  $10^{(0.4e\rho)}$ , where  $e$  is the extinction in magnitudes at  $K$ -band per unit airmass and  $\rho$  is the airmass through which the field was observed. A map of the bad pixels in the array was obtained so that these pixels could be masked out of the frame combination procedure. All the individual frames of each field were registered and combined taking the average for each pixel using the bad pixel mask and a clipping procedure which rejects pixels more than  $4\sigma$  away from the median of the distribution. This gives the final science frame for each field.

### 2.3 Astrometry and identification

Due to uncertainties on scales of a few arcseconds in the telescope pointing, it is necessary to accurately determine the

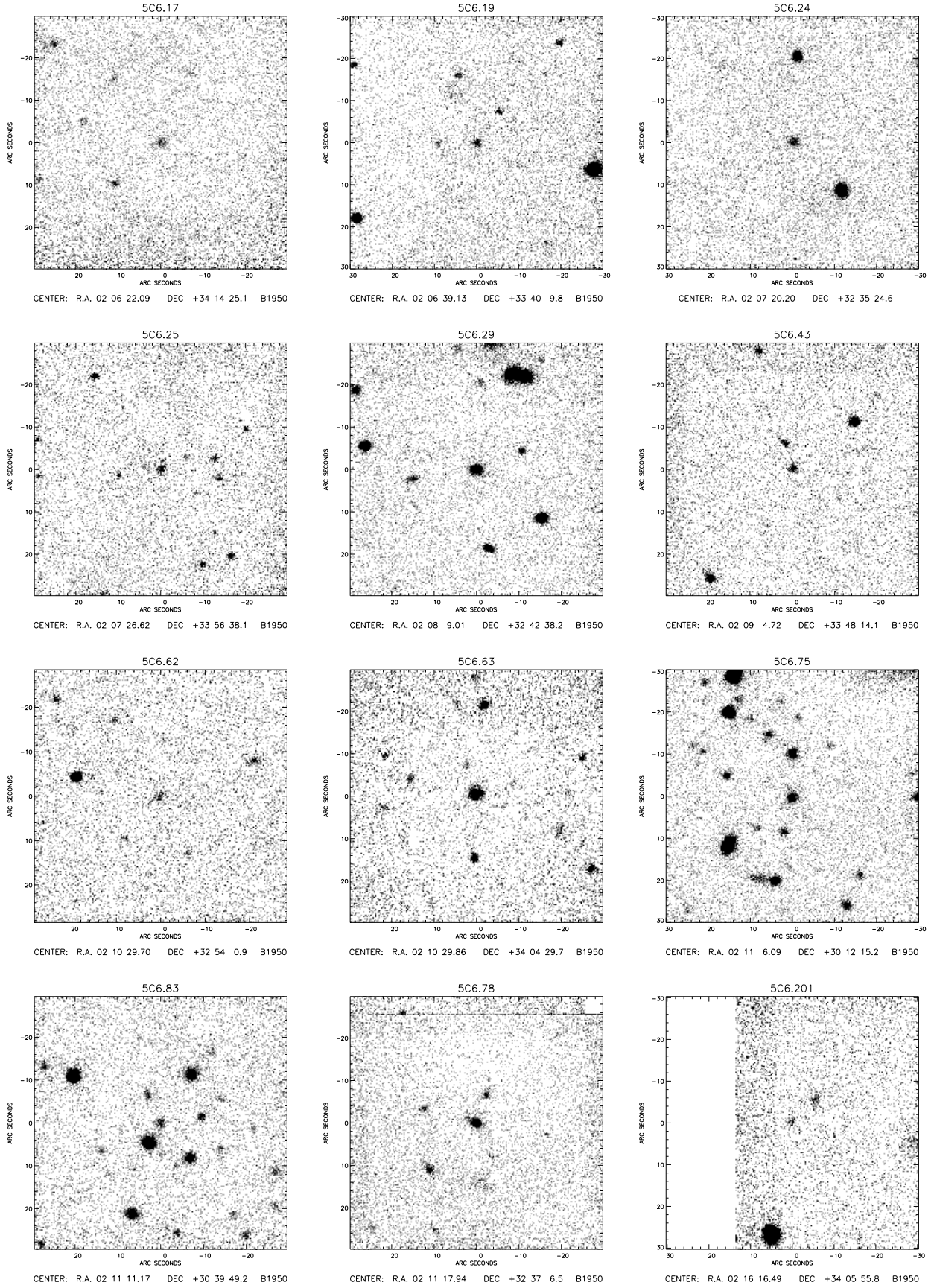
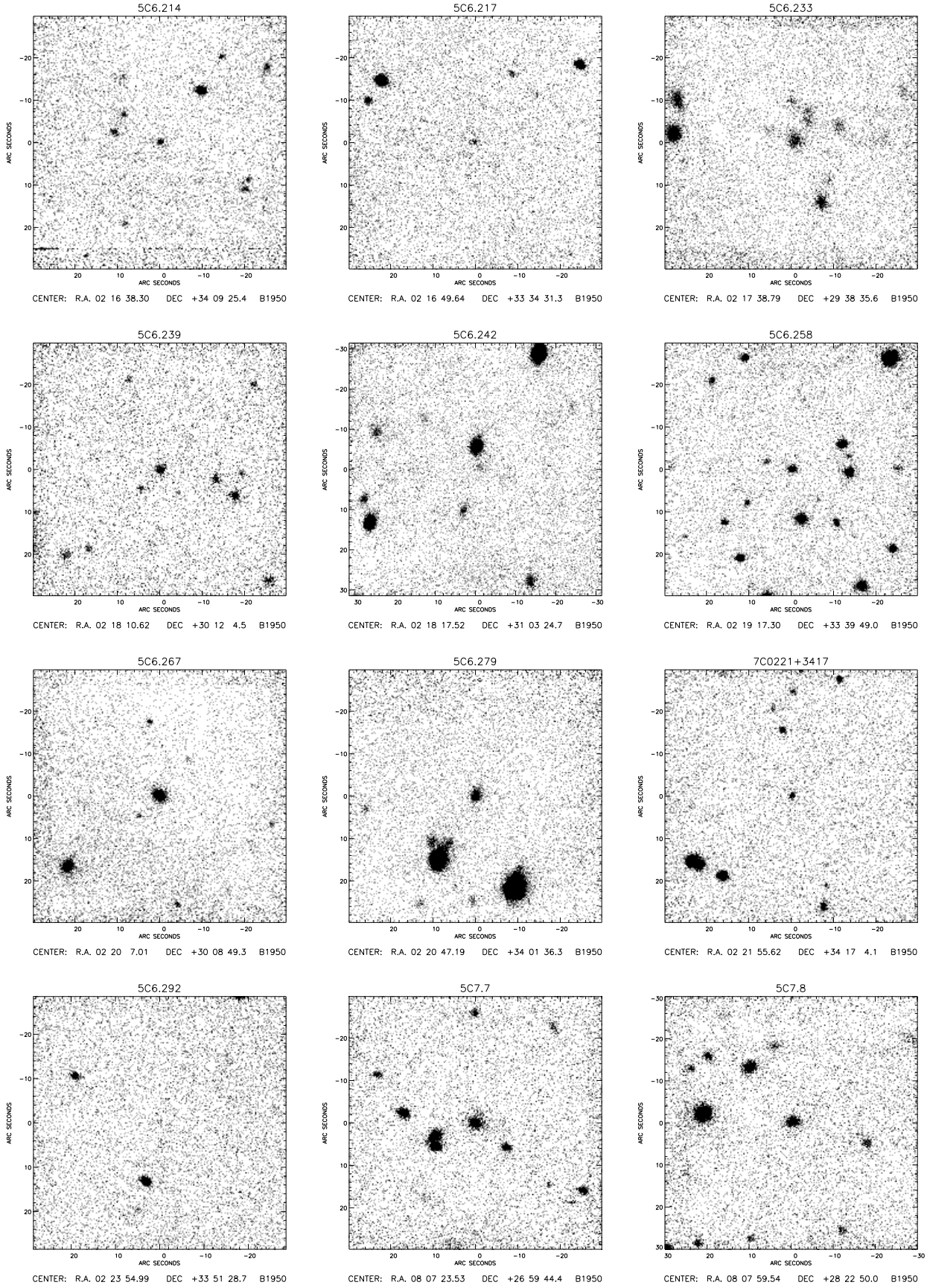


Figure 1.  $K$ -band images of 7C-I radio galaxies. The images are centred on the near-IR identification of the radio source.

Figure 1. (cont.) *K*-band images of 7C-I/II radio galaxies.

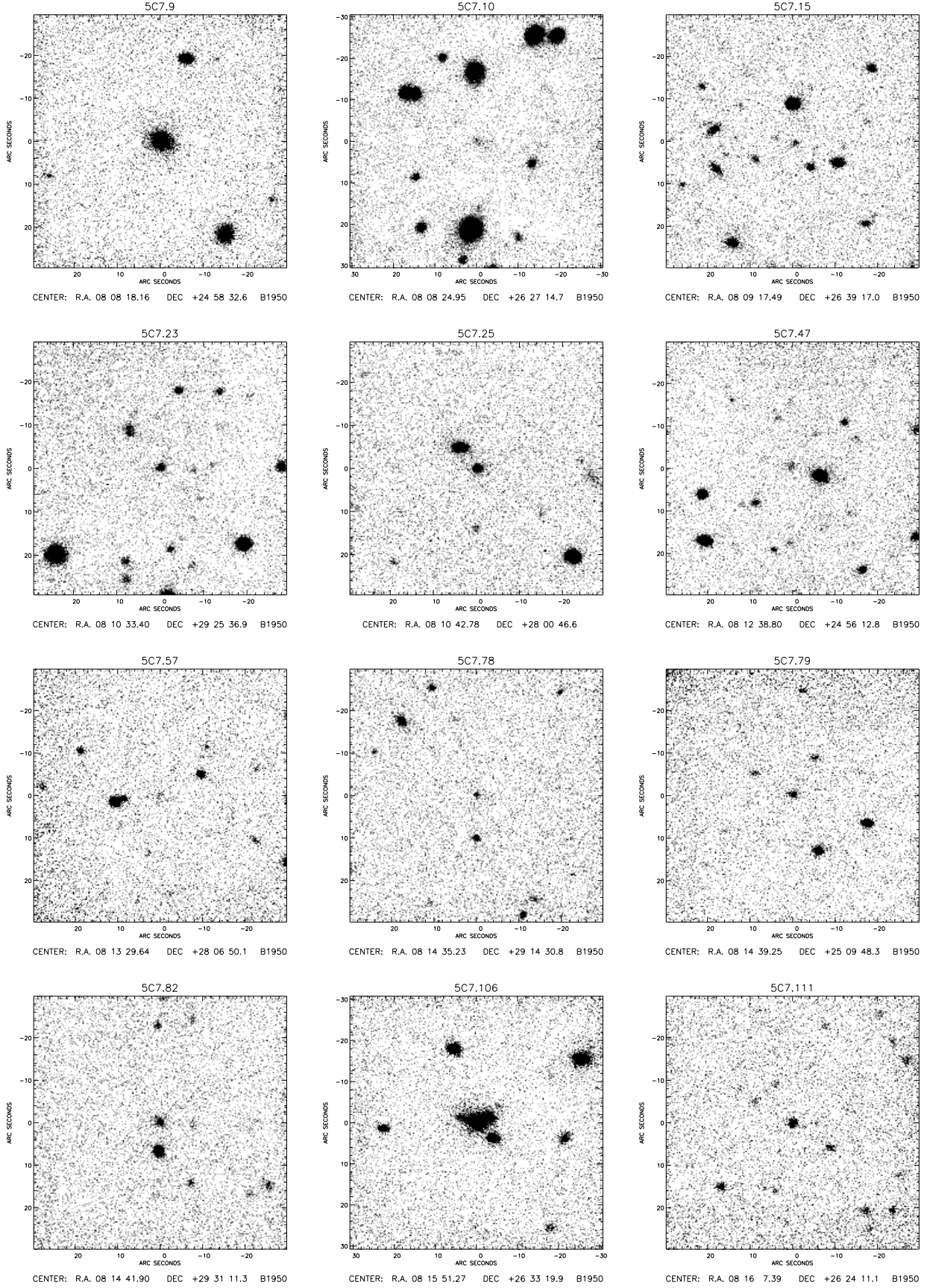
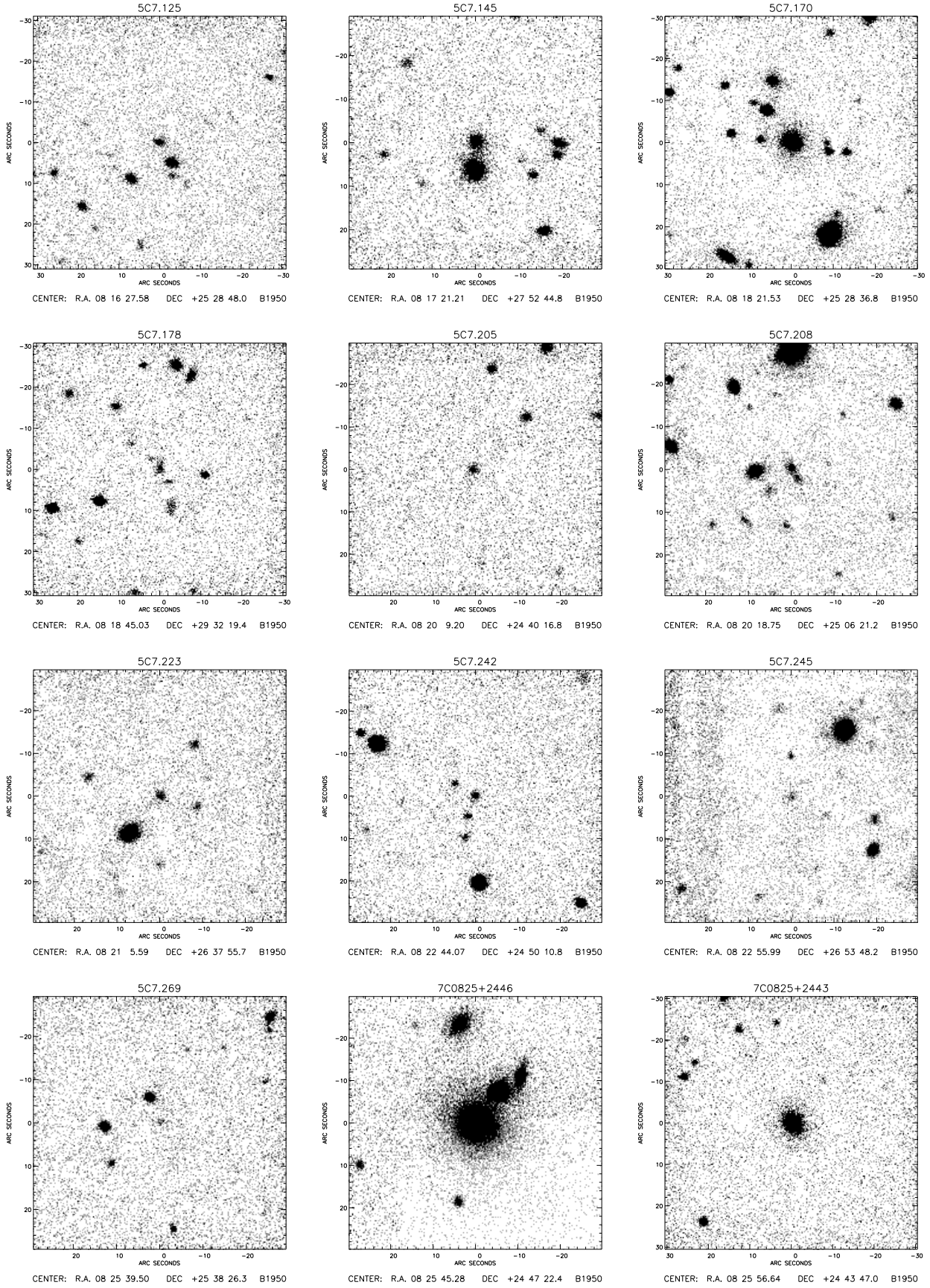
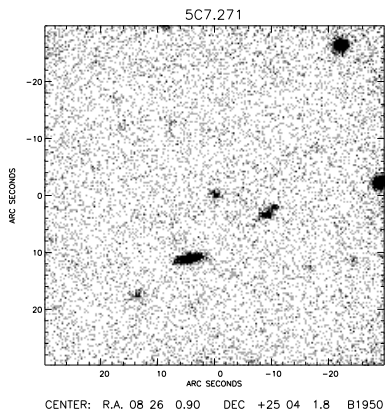


Figure 1. (cont.)  $K$ -band images of 7C-II radio galaxies.



Figure 1. (cont.) *K*-band images of 7C-II radio galaxies.



**Figure 1.** (cont.)  $K$ -band image of a 7C-II radio galaxy.

astrometry of the images. This is crucial in this work, since one must ascertain whether objects detected on the images are the counterparts of the radio sources. To fix the astrometry of the  $K$ -band images, finding charts from the APM catalogue at the Royal Greenwich Observatory, Cambridge, were obtained for each radio source field (Irwin et al. 1994). These charts show objects detected on the red POSS plates to a limit of  $R \approx 20$ . For most fields, one or more stars detected on the  $K$ -band images were also on the APM charts. For cases where 3 or more stars appear on both the image and the chart, the IRAF GASP package was used to determine the plate solution for the image. This takes account of any rotation of the array with respect to North-South (typically of the order of one degree) and determines the pixel scale. The parameters output by this task were entered into the headers of the images, so that any pixel position on the images would be transformed to an accurate position on the sky. For cases where only one or two APM stars were detected on the  $K$ -band image, the plate solution for another image with a good fit on the same observing run was used along with the position of one of the detected stars to fix the astrometry. In a few cases no APM stars were visible on the images, but for these objects wider field  $R$ -band images were available and the astrometry could be achieved by first determining the positions of fainter objects on the  $R$ -band images.

The first step to determining whether the counterparts of the radio sources were detected on the  $K$ -band images was by inspection. The VLA maps resolved the radio sources typically into core and lobe components (Blundell et al. in prep.). Where a core is clearly identifiable, it is usual to find the optical counterpart within an arcsecond or two of this position. Where no core is visible, the counterparts are generally found between the two lobes, often approximately equidistant between the two. Where several objects were close to the expected counterpart position, the radio and  $K$ -band images were overlaid. This enabled a better estimate of the identity of the true counterpart. Subsequent optical spectroscopy of candidates revealed the true identification because of the strong emission lines present in most AGN. Note that in cases where cores and counterparts were both visible, the typical offset between the two was up to 1 arcsec. This is equal to the estimated internal accuracy of

the APM astrometry (Irwin et al. 1994). Any radio galaxies with ambiguous identifications are discussed in the accompanying paper on spectroscopic observations of regions 7C-I and 7C-II of the 7CRS (Willott et al. 2002).

## 2.4 Photometry

Aperture photometry of radio source identifications was performed using the IRAF APPHOT package. The reduction procedure described above does not subtract the background level off the final images. However, the flat-fielding ensures that there is little spatial structure in the background level. To determine the  $K$  magnitudes of detected objects, the local background near each object was measured by averaging over the pixels in an annulus about the object. The inner radius and width of the sky annulus were 5 and 8 arcsec, respectively. Note that any pixels above  $3\sigma$  of the median counts in the sky region are rejected, ensuring that nearby sources do not contaminate the background level. Photometry was performed using three different diameter apertures of 3, 5 and 8 arcsec.

Over the course of each night, several UKIRT faint standard stars were observed (Casali & Hawarden 1992) for photometric calibration. The reduction process used for these standard star observations was identical to that outlined above for the object frames. Aperture photometry of the standard stars gave the zero-point for the images. The zero-points obtained remained fairly constant throughout individual nights, typically with differences of only  $\pm 0.02$  mag. The zero-points obtained at  $K$ -band were  $\approx 22.5$  mag for all the observing runs. The  $K$ -magnitudes and positions of radio source identifications are given in Table 1. Fig. 1 shows greyscale representations of the  $K$ -band images. A summary of the basic information on all the sources in regions 7C-I and 7C-II of the 7CRS is given in Tables 2 and 3.

## 3 THE $K - Z$ RELATION

### 3.1 Data from other samples, and aperture and emission lines corrections

The acquisition of complete  $K$ -band photometry of this sample of radio sources together with  $> 90\%$  spectroscopic redshifts enables us to examine the evolution of the stellar populations of radio galaxies. We do not include in this paper objects which show broad emission lines since they can have a high level of contamination of the  $K$ -band light by non-stellar quasar emission. We do not impose any criteria on the radio structures of the sources considered here, so both FRI and FRII type sources are included. Radio galaxies at  $z < 0.05$  are excluded from our analysis because their large apparent sizes lead to very large aperture corrections from aperture magnitudes.

Lacy et al. (2000) present near-IR data for all radio galaxies at  $z > 0.8$  in the 7C-III region of the 7CRS. Data on all 7C-III galaxies at  $z > 1.2$  are also included here with the 7C-I and 7C-II data described in Sec. 2. This redshift limit was chosen to avoid including objects with data only in the  $J$ -band for which large colour corrections would be necessary to convert to  $K$ -band. Only two of the sixteen sources at  $z > 1.2$  do not have  $K$ -band data and for these

Name	$z$	Date	Exposure Time (s)	Seeing (")	Optical/NIR Position (B1950.0)		$K$ -mag 3" aperture	$K$ -mag 5" aperture	$K$ -mag 8" aperture
5C 6.17	1.05 <sup>‡</sup>	96Feb13	1440	1.4	02 06 22.08	+34 14 25.2	18.45 ± 0.08	17.99 ± 0.08	17.79 ± 0.11
5C 6.19	0.799	96Jul29	540	1.1	02 06 39.11	+33 40 09.8	17.85 ± 0.08	17.51 ± 0.09	17.23 ± 0.11
5C 6.24	1.073	95Jan25	540	1.5	02 07 20.18	+32 35 24.8	17.74 ± 0.13	17.41 ± 0.12	17.25 ± 0.13
5C 6.25	0.706	96Jan21	540	1.1	02 07 26.61	+33 56 38.3	17.88 ± 0.07	17.54 ± 0.07	17.26 ± 0.09
5C 6.29	0.720	96Jan21	1080	1.1	02 08 09.00	+32 42 38.2	16.69 ± 0.02	16.45 ± 0.02	16.35 ± 0.03
5C 6.43	0.775	96Jan21	1080	1.1	02 09 04.70	+33 48 14.3	17.88 ± 0.07	17.69 ± 0.08	17.76 ± 0.14
5C 6.62	1.45 <sup>‡</sup>	97Jan30	540	1.0	02 10 29.69	+32 54 01.0	18.11 ± 0.09	17.70 ± 0.10	17.41 ± 0.12
5C 6.63	0.465	97Aug26	300	1.2	02 10 29.85	+34 04 29.9	16.17 ± 0.06	15.84 ± 0.05	15.71 ± 0.05
5C 6.75	0.775	96Jan21	1620	1.2	02 11 06.09	+30 12 15.2	17.52 ± 0.04	17.22 ± 0.04	17.06 ± 0.05
5C 6.83	1.80 <sup>‡</sup>	97Jan29	1080	1.3	02 11 11.17	+30 39 49.3	18.30 ± 0.07	18.12 ± 0.10	nbo
5C 6.78	0.263	97Jan30	180	1.0	02 11 17.94	+32 37 06.6	15.95 ± 0.02	15.65 ± 0.03	15.51 ± 0.04
5C 6.201	0.595	97Aug26	150	1.1	02 16 16.49	+34 05 56.1	17.71 ± 0.11	17.47 ± 0.15	17.45 ± 0.24
5C 6.214	0.595	97Jan30	300	1.0	02 16 38.28	+34 09 25.6	17.49 ± 0.07	17.20 ± 0.09	17.25 ± 0.16
5C 6.217	1.410	96Jul29	540	1.1	02 16 49.62	+33 34 31.5	18.52 ± 0.12	18.34 ± 0.17	18.02 ± 0.21
5C 6.233	0.560	95Mar01	1080	1.4	02 17 38.79	+29 38 35.6	17.83 ± 0.04	17.22 ± 0.04	17.03 ± 0.06
5C 6.239	0.805	96Jan21	540	1.2	02 18 10.60	+30 12 04.5	17.48 ± 0.04	17.28 ± 0.05	17.24 ± 0.08
5C 6.242	1.90 <sup>‡</sup>	96Feb13	2700	1.6	02 18 17.50	+31 03 24.8	18.77 ± 0.07	18.52 ± 0.07	nbo
5C 6.258	0.752	96Jan21	1620	1.1	02 19 17.29	+33 39 49.1	17.95 ± 0.04	17.80 ± 0.05	17.69 ± 0.08
5C 6.267	0.357	97Jan30	180	1.0	02 20 07.00	+30 08 49.5	15.37 ± 0.01	15.05 ± 0.01	14.92 ± 0.02
5C 6.279	0.473	96Feb13	660	1.6	02 20 47.17	+34 01 36.4	16.92 ± 0.03	16.53 ± 0.03	16.36 ± 0.04
7C 0221+3417	0.852	97Jan30	540	1.1	02 21 55.60	+34 17 04.1	18.02 ± 0.08	17.76 ± 0.10	17.48 ± 0.13
5C 6.292	1.241	96Jul29	540	1.1	02 23 54.99	+33 51 28.9	19.82 ± 0.39	19.27 ± 0.40	19.37 ± 0.73
5C 7.7	0.435	96Mar11	540	1.1	08 07 23.52	+26 59 44.5	16.33 ± 0.02	15.96 ± 0.02	15.73 ± 0.03
5C 7.8	0.673	95Mar01	540	1.4	08 07 59.52	+28 22 50.1	16.92 ± 0.02	16.61 ± 0.02	16.48 ± 0.04
5C 7.9	0.233	96Mar11	270	1.2	08 08 18.14	+24 58 32.7	14.93 ± 0.01	14.54 ± 0.01	14.34 ± 0.01
5C 7.10	2.185	95Mar01	2700	1.2	08 08 24.94	+26 27 14.8	19.44 ± 0.10	18.95 ± 0.10	18.80 ± 0.15
5C 7.15	2.433	96Jan21	900	1.1	08 09 17.49	+26 39 17.3	18.86 ± 0.11	18.56 ± 0.14	18.69 ± 0.27
5C 7.23	1.098	95Mar01	1620	1.1	08 10 33.38	+29 25 37.2	18.34 ± 0.05	18.07 ± 0.06	17.98 ± 0.09
5C 7.25	0.671	95Jan25	540	1.2	08 10 42.77	+28 00 46.6	17.16 ± 0.09	16.83 ± 0.08	16.61 ± 0.08
5C 7.47	1.70 <sup>‡</sup>	96Jan21	4320	1.1	08 12 38.78	+24 56 13.0	19.52 ± 0.10	19.28 ± 0.13	19.17 ± 0.19
5C 7.57	1.622	96Feb13	540	1.0	08 13 29.64	+28 06 50.1	19.15 ± 0.18	18.59 ± 0.19	18.76 ± 0.41
5C 7.78	1.151	97Jan30	540	0.7	08 14 35.21	+29 14 31.1	18.30 ± 0.09	17.91 ± 0.11	17.75 ± 0.16
5C 7.79	0.608	96Mar11	270	1.1	08 14 39.24	+25 09 48.5	17.47 ± 0.05	17.18 ± 0.07	17.12 ± 0.11
5C 7.82	0.918	97Jan29	540	1.1	08 14 41.90	+29 31 11.5	17.45 ± 0.05	17.06 ± 0.05	17.01 ± 0.09
5C 7.106	0.264	96Mar11	270	1.0	08 15 51.26	+26 33 20.1	15.21 ± 0.01	nbo	nbo
5C 7.111	0.628	96Feb13	540	1.2	08 16 07.39	+26 24 11.1	17.15 ± 0.03	17.04 ± 0.04	16.92 ± 0.06
5C 7.125	0.801	96Mar10	1080	1.0	08 16 27.58	+25 28 48.2	17.91 ± 0.04	17.61 ± 0.05	17.40 ± 0.07
5C 7.145	0.343	96Mar11	270	1.1	08 17 21.19	+27 52 45.0	16.06 ± 0.01	15.65 ± 0.01	15.35 ± 0.02
5C 7.170	0.268	96Mar11	270	1.1	08 18 21.53	+25 28 36.9	15.00 ± 0.01	14.57 ± 0.01	14.33 ± 0.01
5C 7.178	0.246	96Mar11	270	1.1	08 18 45.02	+29 32 19.4	17.63 ± 0.06	17.36 ± 0.08	nbo
5C 7.205	0.710	95Mar01	540	1.3	08 20 09.19	+24 40 17.1	17.82 ± 0.05	17.44 ± 0.06	17.26 ± 0.08
5C 7.208	2.00 <sup>‡</sup>	95Mar01	1620	1.2	08 20 18.74	+25 06 21.4	18.06 ± 0.04	17.60 ± 0.04	nbo
5C 7.223	2.092	95Mar01	2700	1.2	08 21 05.57	+26 37 55.8	18.76 ± 0.05	18.41 ± 0.06	18.27 ± 0.09
5C 7.242	0.992	96Feb13	480	1.1	08 22 44.06	+24 50 11.0	17.60 ± 0.05	17.39 ± 0.06	17.24 ± 0.09
5C 7.245	1.61 <sup>‡</sup>	95Mar01	2700	1.2	08 22 55.99	+26 53 48.2	19.19 ± 0.08	18.76 ± 0.09	18.51 ± 0.11
5C 7.269	2.218	97Jan29	1080	0.9	08 25 39.48	+25 38 26.5	19.18 ± 0.14	18.82 ± 0.16	18.59 ± 0.22
7C 0825+2446	0.086	97Jan30	540	1.3	08 25 45.26	+24 47 22.5	13.68 ± 0.01	13.09 ± 0.01	12.72 ± 0.01
7C 0825+2443	0.243	96Mar11	270	1.1	08 25 56.62	+24 43 47.0	14.97 ± 0.01	14.53 ± 0.01	14.30 ± 0.01
5C 7.271	2.224	96Jan21	2620	1.1	08 26 00.89	+25 04 01.8	18.96 ± 0.08	18.77 ± 0.12	18.73 ± 0.19

**Table 1.** Log of  $K$ -band observations of the 7C-I and 7C-II radio galaxies using IRCAM3 on the UKIRT. Errors on magnitudes do not include systematic errors due to zero-point uncertainties (typically  $\pm 0.02$  mag). ‘nbo’ in the aperture magnitude column denotes that for these sources contamination of the  $K$ -band flux by a nearby object prevents an accurate measurement. <sup>‡</sup>These redshifts are not from optical spectroscopy, but have been estimated from optical/near-IR colours and near-infrared spectroscopy (Willott et al. 2001).

objects at  $z \approx 1.5$  we assume a colour of  $H - K = 0.9$  to convert from the  $H$ -band magnitudes in Lacy et al.

In addition we can combine our data with those from brighter complete samples to search for any correlation of near-IR luminosity with radio luminosity. The two complete flux-density limited samples selected at a similar radio frequency to the 7CRS are the 3CRR and 6CE samples.  $K$ -band photometry of 3CRR sources is taken from Lilly &

Longair (1984), Best et al. (1998), Simpson, Ward & Wall (2000), de Vries et al. (1998), Hutchings & Neff (1997), Rawlings et al. (1996) and Stockton, Canalizo & Ridgway (1999) using the more recent data where multiple measurements exist. Note that this does not include every radio galaxy in the 3CRR sample. 27 out of the 96 3CRR radio galaxies with  $z \geq 0.05$  do not have  $K$ -band photometry in these publications. We assume that the observed sample is repre-



(1)	(2)	(3)	(4)	(5)	(6)	(7)
Name	$\log_{10} L_{151}$	Cl	$K$	$z$	Line	$\log_{10} L_{\text{line}}$
5C 6.5	26.31	Q	$16.26 \pm 0.05$ (5)	1.038	[OII]†	35.62
5C 6.8	26.83	Q	$16.28 \pm 0.06$ (5)	1.213	[OIII]	35.85
5C 6.17	26.56	G	$17.79 \pm 0.11$ (8)	1.05 <sup>‡</sup>	H $\alpha$	<35.21
5C 6.19	26.51	G	$17.23 \pm 0.11$ (8)	0.799	[OII]	34.78
5C 6.24	26.68	G	$17.25 \pm 0.13$ (8)	1.073	[OII]	35.55
5C 6.25	26.07	G	$17.26 \pm 0.09$ (8)	0.706	[OII]	35.34
5C 6.29	25.94	G	$16.35 \pm 0.03$ (8)	0.720	[OII]	35.03
5C 6.33	26.64	Q	$18.23 \pm 0.19$ (5)	1.496	[OII]†	35.06
5C 6.34	27.12	Q	$15.94 \pm 0.04$ (5)	2.118	[OII]†	36.70
5C 6.39	26.59	Q	$17.87 \pm 0.08$ (5)	1.437	[NeV]	35.37
5C 6.43	26.16	G	$17.76 \pm 0.14$ (8)	0.775	[OII]	34.04
5C 6.62	26.92	G	$17.41 \pm 0.12$ (8)	1.45 <sup>‡</sup>	H $\alpha$	<35.73
5C 6.63	25.66	G	$15.71 \pm 0.05$ (8)	0.465	[OII]	33.95
5C 6.75	25.93	G	$17.06 \pm 0.05$ (8)	0.775	[OII]	34.70
5C 6.83	27.20	G	$15.51 \pm 0.04$ (8)	1.80 <sup>‡</sup>	H $\alpha$	<35.81
5C 6.78	25.62	G	$18.12 \pm 0.10$ (5)	0.263	[OIII]	35.01
5C 6.95	27.55	Q	$16.04 \pm 0.04$ (5)	2.877	[OII]†	35.91
5C 6.160	26.88	Q	$17.95 \pm 0.14$ (5)	1.624	[OIII]	36.58
5C 6.201	26.12	G	$17.45 \pm 0.24$ (8)	0.595	[OIII]	34.39
5C 6.214	25.97	G	$17.25 \pm 0.16$ (8)	0.595	[OII]	34.19
5C 6.217	27.13	G	$18.02 \pm 0.21$ (8)	1.410	CIII]	34.91
5C 6.233	26.07	G	$17.03 \pm 0.06$ (8)	0.560	[OII]	34.39
5C 6.237	27.11	Q	$15.76 \pm 0.03$ (5)	1.620	[OIII]	36.69
5C 6.239	26.19	G	$17.24 \pm 0.08$ (8)	0.805	[OII]	35.16
5C 6.242	27.06	G	$18.52 \pm 0.07$ (5)	1.90 <sup>‡</sup>	H $\alpha$	<36.09
5C 6.251	26.70	Q	$17.66 \pm 0.11$ (5)	1.665	[NeIV]	35.58
5C 6.258	25.99	G	$17.69 \pm 0.08$ (8)	0.752	[OII]	34.61
5C 6.264	26.27	Q	$16.16 \pm 0.04$ (5)	0.831	[OII]	35.08
5C 6.267	25.16	G	$14.92 \pm 0.02$ (8)	0.357	[OII]	34.88
5C 6.279	25.54	G	$16.36 \pm 0.04$ (8)	0.473	[OII]	34.83
5C 6.282	27.03	Q	$18.20 \pm 0.18$ (5)	2.195	[OII]†	35.52
7C 0221+3417	26.79	G	$17.48 \pm 0.13$ (8)	0.852	[OII]	34.69
5C 6.286	26.65	Q	$17.62 \pm 0.20$ (3)	1.339	[OIII]	<35.35
5C 6.288	27.60	Q	$18.28 \pm 0.12$ (4)	2.982	Ly $\alpha$	36.68
5C 6.287	27.57	Q	$16.11 \pm 0.04$ (5)	2.296	[OII]†	36.78
5C 6.291	27.56	Q	$16.06 \pm 0.03$ (5)	2.910	Ly $\alpha$	37.10
5C 6.292	26.72	G	$19.37 \pm 0.73$ (8)	1.241	[OII]	35.93

**Table 2.** A summary of key information on the 7C-I sample. Full details of spectroscopic observations are given in Willott et al. (1998) for the quasars and broad-lined radio galaxies and Willott et al. (2002) for the narrow-line radio galaxies. Note that the cosmological parameters assumed here to calculate the radio and emission line luminosities differ from those used in many of our previous papers. **Column 1:** Name of the radio source. Note that most of the names begin with 5C 6 because they were originally catalogued in the 5C survey in this region (Pearson & Kus 1978). **Column 2:**  $\log_{10}$  of the rest-frame 151-MHz radio luminosity in units of  $\text{W Hz}^{-1} \text{sr}^{-1}$ . **Column 3:** Classification, Q=quasar, B=broad-line radio galaxy, G=narrow-line radio galaxy following the prescription of Willott et al. (1998). **Column 4:**  $K$ -band magnitude of the radio source ID and photometric error. The number in brackets is the diameter in arcsec of the photometric aperture. **Column 5:** Redshift. <sup>‡</sup>These redshifts are not from optical spectroscopy, but have been estimated from optical/near-IR colours and near-infrared spectroscopy (Willott et al. 2001). **Column 6:** Prominent narrow emission line in the existing spectra. †indicates that the line has not been observed for this quasar but the line luminosity has been estimated assuming a typical [OII] equivalent width of 10 Å. **Column 7:**  $\log_{10}$  of the line luminosity in units of W, a < denotes that the line is not detected and an upper limit is quoted.

sentative and that no biases are introduced by the missing sources. A compilation of data for the complete 6CE sample is given in Rawlings et al. (2001). We also include data from the filtered 6C\* sample because the linear size and spectral index criteria do not seem to affect the position on the  $K - z$  relation and this sample has very high spectroscopic redshift completeness (Jarvis et al. 2001a,b). The total numbers of  $z \geq 0.05$  radio galaxies in each of the samples with  $K$ -band data are 69 in 3CRR, 47 in 6CE, 65 in 7CRS and 23 in 6C\* (total 204). The data for all the samples used in this paper are available on-line at <http://www-astro.physics.ox.ac.uk/~cjlw/kz/kz.html>.

$K$ -band magnitudes of radio galaxies in the 7C-I, 7C-II and 6C\* samples are quoted in 3,5 and 8 arcsec apertures. However, for the 3CRR, 6CE and 7C-III radio galaxies the data are given in various apertures. We apply the same procedure as in Jarvis et al. (2001a) to convert from apparent angular size aperture magnitudes to standard 64 kpc metric apertures to be consistent with previous studies. As highlighted by Eales et al. (1993), the strong emission lines of the most powerful radio sources can provide significant flux contamination at  $K$ -band, particularly at  $z \approx 2$  where the H $\alpha$  line lies in the  $K$ -band. Jarvis et al. (2001a) accounted for the emission line contribution by assuming that

(1)	(2)	(3)	(4)	(5)	(6)	(7)
Name	$\log_{10} L_{151}$	Cl	$K$	$z$	Line	$\log_{10} L_{\text{line}}$
5C 7.7	25.57	G	$15.73 \pm 0.03$ (8)	0.435	[OII]	34.28
5C 7.8	26.36	G	$16.48 \pm 0.04$ (8)	0.673	[OII]	34.97
5C 7.9	25.36	G	$14.34 \pm 0.01$ (8)	0.233	[OIII]	35.52
5C 7.10	27.54	G	$18.80 \pm 0.15$ (8)	2.185	Ly $\alpha$	36.95
7C 0808+2854	27.13	Q	$16.06 \pm 0.04$ (5)	1.883	[OIII]	36.76
5C 7.15	27.35	G	$18.69 \pm 0.27$ (8)	2.433	Ly $\alpha$	36.25
5C 7.17	26.20	B	$17.37 \pm 0.07$ (5)	0.936	[OII]	35.25
5C 7.23	26.63	G	$17.98 \pm 0.09$ (8)	1.098	[OII]	35.16
5C 7.25	25.77	G	$16.61 \pm 0.08$ (8)	0.671	[OII]	34.77
5C 7.47	26.79	G	$19.17 \pm 0.19$ (8)	1.70 <sup>†</sup>	MgII	<34.98
5C 7.57	26.78	G	$18.76 \pm 0.41$ (8)	1.622	CIII]	35.02
5C 7.70	27.75	Q	$17.48 \pm 0.09$ (5)	2.617	[OII] <sup>†</sup>	36.02
5C 7.78	26.99	G	$17.75 \pm 0.16$ (8)	1.151	[OII]	35.47
5C 7.79	25.76	G	$17.12 \pm 0.11$ (8)	0.608	[OII]	34.24
5C 7.82	26.28	G	$17.01 \pm 0.09$ (8)	0.918	[OII]	34.86
5C 7.85	26.63	Q	$16.24 \pm 0.03$ (5)	0.995	[OII]	35.18
5C 7.87	27.17	Q	$18.74 \pm 0.22$ (5)	1.764	[OII] <sup>†</sup>	35.21
5C 7.95	26.65	Q	$16.61 \pm 0.03$ (5)	1.203	[OIII]	36.17
5C 7.106	25.27	G	$15.21 \pm 0.01$ (3)	0.264	[OIII]	<33.82
5C 7.111	26.29	G	$16.92 \pm 0.06$ (8)	0.628	[OII]	34.70
5C 7.118	26.05	B	$15.75 \pm 0.03$ (5)	0.527	[OIII]	34.97
5C 7.125	26.14	G	$17.40 \pm 0.07$ (8)	0.801	[OII]	34.63
5C 7.145	25.31	G	$15.35 \pm 0.02$ (8)	0.343	[OII]	<33.94
5C 7.170	25.18	G	$14.33 \pm 0.01$ (8)	0.268	[OIII]	<33.68
5C 7.178	25.14	G	$17.36 \pm 0.08$ (5)	0.246	[OIII]	32.85
5C 7.194	27.29	Q	$15.91 \pm 0.03$ (5)	1.738	[NeIV]	36.07
5C 7.195	27.12	Q	$17.71 \pm 0.05$ (5)	2.034	Ly $\alpha$	37.04
5C 7.205	26.34	G	$17.26 \pm 0.08$ (8)	0.710	[OII]	35.20
5C 7.208	27.27	G	$17.60 \pm 0.04$ (5)	2.00 <sup>†</sup>	H $\alpha$	<35.61
5C 7.223	27.06	G	$18.27 \pm 0.09$ (8)	2.092	Ly $\alpha$	36.71
5C 7.242	26.21	G	$17.24 \pm 0.09$ (8)	0.992	[OII]	34.71
5C 7.245	27.22	G	$18.51 \pm 0.11$ (8)	1.61 <sup>†</sup>	H $\alpha$	35.92
7C 0825+2930	26.95	Q	$17.55 \pm 0.15$ (4)	2.315	[OII] <sup>†</sup>	35.96
5C 7.269	27.21	G	$18.59 \pm 0.22$ (8)	2.218	Ly $\alpha$	36.51
7C 0825+2446	24.85	G	$12.72 \pm 0.01$ (8)	0.086	[OIII]	<32.82
7C 0825+2443	24.93	G	$14.30 \pm 0.01$ (8)	0.243	[OIII]	<33.45
5C 7.271	27.06	G	$18.73 \pm 0.19$ (8)	2.224	CIII]	34.96

**Table 3.** A summary of key information on the 7C-II sample in the same format as Table 2. Most of the names begin with 5C 7 because they were originally catalogued in the 5C survey in this region (Pearson & Kus 1978). Note that the 3CRR source 3C 200 should technically be included in the 7C-II sample, since it is contained within this region of sky and has a 151 MHz flux-density above the limit.

sources follow the emission line – radio correlation of Willott (2001). We adopt this method in this paper and correct the  $K$ -magnitudes of all sources for the expected emission line flux.

### 3.2 The evolution of the stellar hosts of radio galaxies

In Fig. 2 we show the near-infrared Hubble diagram of  $K$ -magnitude versus  $z$  for the 7CRS, 6CE, 6C\* and 3CRR samples. The solid line is the best-fit second order polynomial relationship between  $K$  and  $\log_{10} z$  for all the data (calculated by minimizing the square of the residuals in  $K$ ). Although in Sec. 4 we will show that the different samples do follow slightly different  $K - z$  relations, the weakness of this effect and the relative lack of evolution of the difference means that we can include all the data here to define the  $K - z$  relation for all powerful radio galaxies. The best-fit relation is

$$K = 17.37 + 4.53 \log_{10} z - 0.31(\log_{10} z)^2 \quad (1)$$

Eales et al. (1997) found that the dispersion in the  $K - z$  relation for the 6CE sample increased markedly at redshifts  $z > 2$  and proposed that this was revealing the epoch of formation of massive ellipticals. A similar effect was found by Lacy et al. (2000) including the 7C-III data and high redshift radio galaxies from the literature. However Jarvis et al. (2001a) found no increase in the dispersion up to  $z \sim 3$  for the combination of the 6CE and 6C\* samples. We have evaluated the dispersion about our best-fit relation as a function of redshift. We find a standard deviation  $\sigma$  that is approximately constant at all redshifts:  $\sigma = 0.57$  at  $0.05 < z < 1$ ,  $\sigma = 0.60$  at  $1 < z < 2$ ,  $\sigma = 0.59$  at  $2 < z < 3$ . This appears to be in agreement with the results of Jarvis et al. (2001a), but we caution that the highest redshift bin does not include any 3C sources so the correlation between radio luminosity and  $K$ -magnitude (Sec. 4) may be increasing the dispersion in the lower redshift bins (although Jarvis et al. find comparable dispersions in the 6C data alone at these

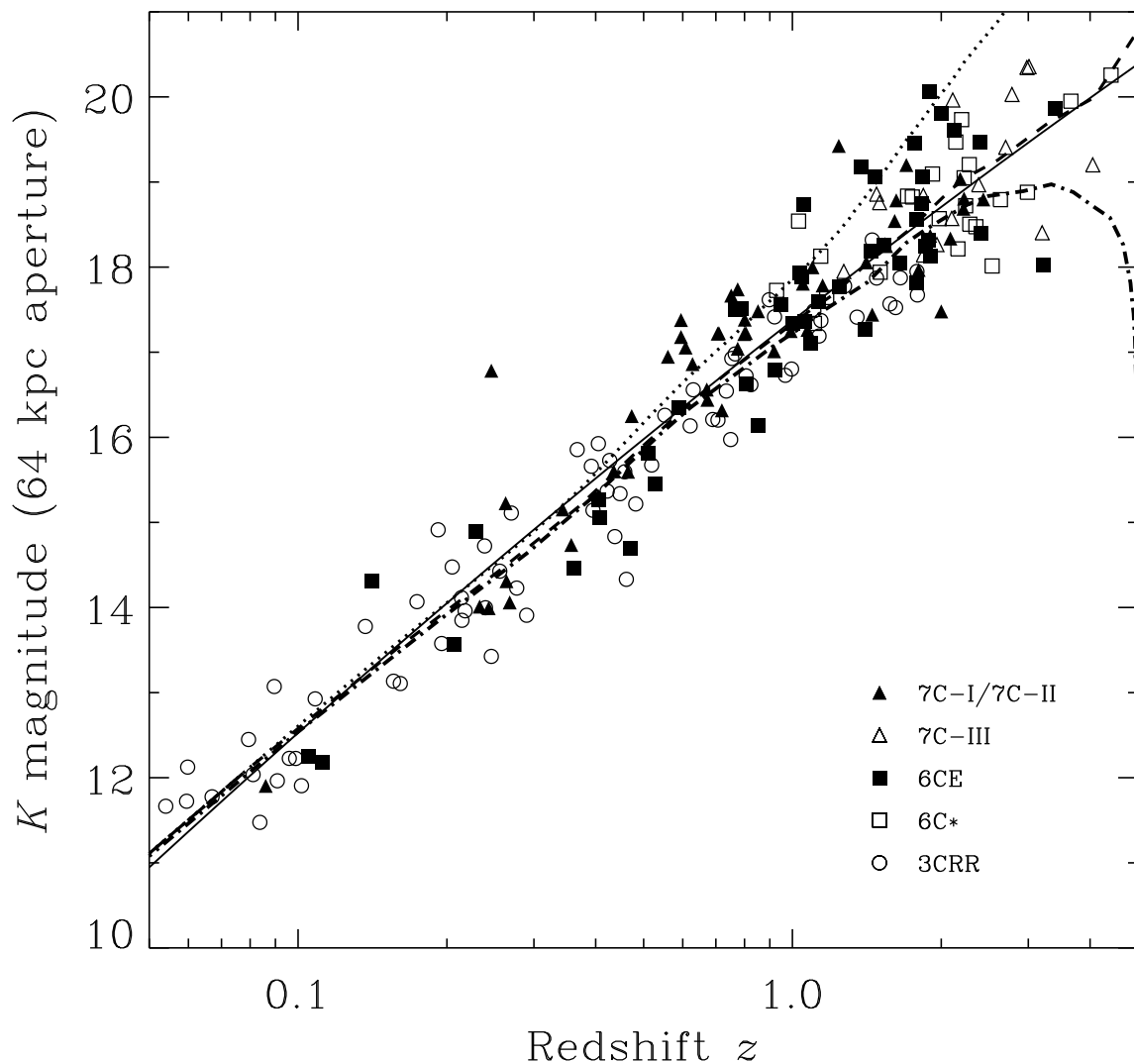


**Figure 2.** Aperture and emission line corrected  $K$ -band magnitude versus redshift for radio galaxies from the 7CRS, 6CE, 6C\* and 3CRR complete samples. The solid curve is the best-fit second order polynomial relationship between  $K$  and  $\log_{10} z$  for all the data. This is remarkably similar to the apparent  $K$ -magnitude evolution of a galaxy of local luminosity  $3 L_{\star}$  which forms all its stars in an instantaneous burst at  $z_f = 10$  (dashed line). A similar model with  $z_f = 5$  (dot-dashed line) predicts galaxies are much more luminous at  $z > 3$ . The no-evolution model for a  $3 L_{\star}$  galaxy (dotted) provides a poor fit to the  $z > 1$  data.

lower redshifts). One of the 7CRS galaxies at  $z = 0.246$  is much fainter than all other radio galaxies at this redshift and is the only major outlier from the  $K - z$  relation. This source, 5C 7.178, is discussed further in Willott et al. (2002).

Also plotted on Fig. 2 are curves showing the evolution in apparent  $K$ -magnitude for several model galaxies determined using GISEL96 (Bruzual & Charlot 2002). The upper curve (dotted line) is for a model galaxy with luminosity  $3 L_{\star}$  (assuming  $M_K^{\star} = -24.3$  for local ellipticals from Kochanek et al. 2000) which includes the  $k$ -correction but no evolution in the stellar population. At all redshifts, the spectrum of the model galaxy is that of a 13 Gyr old instantaneous burst with solar metallicity (note that this violates constraints from the age of the Universe at high redshifts). As first shown by Lilly & Longair (1984), at  $z > 1$ , ra-

dio galaxies are typically more luminous than their local counterparts, implying significant evolution in their stellar populations. This is evident in Fig. 2 by the poor fit of the non-evolving model.

We have also evaluated the evolution in  $K$ -magnitude for evolving stellar population models which formed all their stars in an instantaneous burst at high redshift. Evolving models for a  $3 L_{\star}$  galaxy with formation redshifts of  $z_f = 5$  (dot-dashed) and  $z_f = 10$  (dashed) are also plotted on Fig. 2. The  $z_f = 10$  curve is remarkably close to the best-fit relation over the whole redshift range, indicating the mean luminosity of radio galaxies is  $3 L_{\star}$ <sup>1</sup>. However at least some of the  $z > 3$  radio galaxies lie closer to the  $z_f = 5$  curve. It is also worth recalling that in modern theoretical models for galaxy formation (e.g. Somerville & Primack 1999;

Cole et al. 2000), there is a significant amount of merging at high-redshifts. This means that objects which appear to follow the  $z_f = 10$  passive evolution curve could equally well be less massive galaxies with a more recent star-formation epoch. We will not discuss the evolutionary implications of the  $K - z$  relation in detail here, since these issues have recently been discussed for subsets of these data by Jarvis et al. (2001a) and Inskip et al. (2002). We note that Inskip et al. stated that the passive evolution model with  $z_f = 10$  in a  $\Omega_M = 0.3, \Omega_\Lambda = 0.7$  cosmology did not provide a good fit to their combined 3CRR and 6CE sample. The deviations of their model from the binned data were only  $\approx 0.4$  magnitudes at  $z = 0.5, z = 1$  and  $z = 2$ , i.e. less than the standard deviation in the data and formally consistent with the evolution over the redshift range  $0.5 < z < 2$ . Their differing result from ours is due to the new data presented here, our emission line corrections and a slightly different low-redshift normalization. We conclude that the passive evolution model is consistent with the  $K - z$  relation in a  $\Lambda$ -dominated cosmology, especially given the further complications to be discussed in Sec. 4.

#### 4 RADIO-LUMINOSITY DEPENDENCE OF THE STELLAR HOST LUMINOSITY

There is a simple explanation of why we may expect to find that the stellar luminosities of radio galaxies are correlated with radio luminosity. In essence, this comes down to the fact that more massive objects are generally more luminous. In this case there are several observed correlations that can be used to specify the relationship between stellar and radio luminosity. First, the stellar luminosity of ellipticals is known to correlate almost linearly with the central black hole mass (Magorrian et al. 1988), presumably because the stellar luminosity is very closely related to the stellar mass and there is a tight correlation between host and black hole masses (Gebhardt et al. 2000; Ferrarese & Merritt 2000). The radio luminosity is found to be linearly related to the narrow emission line luminosity (Willott 2001) and therefore presumably to the UV ionizing luminosity (Rawlings & Saunders 1991; Willott et al. 1999). The UV ionizing luminosity draws its power from the accretion of material onto the supermassive black hole. Therefore any correlation between stellar and radio luminosities is likely to have its cause in the fact that both properties correlate positively with the black hole mass. This means that by measuring the strength of any correlation between the stellar and radio luminosities, we can estimate the range of black hole masses in high-redshift radio galaxies.

To investigate the correlation between the stellar and radio luminosities we determine the residuals for each object about the best fitting  $K - z$  relation presented in Sec.

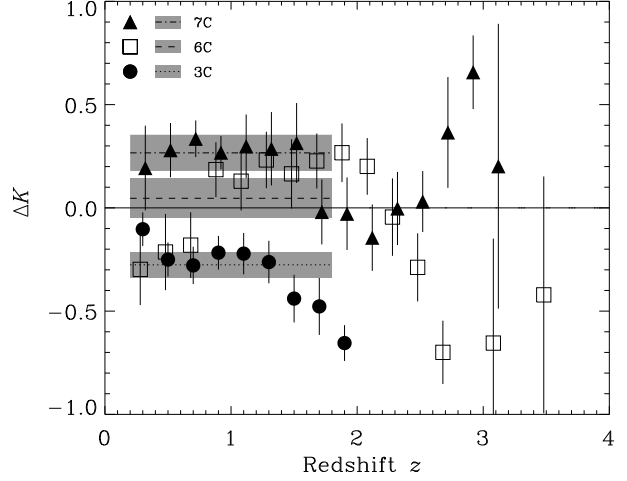


**Figure 3.** Residuals from the best fit to the  $K - z$  relationship ( $\Delta K = K - K_{\text{fit}}$ ) against redshift. The data for each sample have been binned in bins of width  $\Delta z = 0.6$  and the error bars show the standard errors which are correlated as described in Sec. 4. Only bins containing 3 or more sources are plotted. The 6C and 7C bins are shown offset from their true central redshifts by  $\pm 0.02$  for clarity. The dot-dashed, dashed and dotted lines show the mean value of  $\Delta K$  over the redshift range  $0.2 < z < 1.8$  for the 7C, 6C and 3C samples, respectively. The grey shading about these lines show the  $\pm 1\sigma$  standard errors about the means.

3.2 and Fig. 2. We do not bin the sources in terms of radio luminosity since the sources from different samples span a range of redshifts at a given luminosity and we wish to investigate the evolutionary dependence of any correlation. However, because the samples are radio flux-limited the median flux-density of 6C sources is  $\approx 7$  times fainter than that of 3C sources and the 7C sources a further factor of  $\approx 2.5$  times fainter than 6C. Therefore the radio luminosities of sources at a given redshift typically differ by these amounts and we determine the mean residual for each sample as a function of redshift. To obtain a large enough number of objects per sample per bin, the bins in redshift have width  $\Delta z = 0.6$ . To avoid spurious results due to the choice of binning, we have evaluated the mean residual per sample per bin for a range of bins from  $0 < z < 0.6$  to  $3.2 < z < 3.8$  with steps of 0.2 in  $z$ . This does mean that neighbouring points are correlated but gives a more accurate measure of the true differences between the samples as a function of epoch.

In Fig. 3 we plot the mean  $K$ -magnitude residuals as a function of redshift for the three sets of samples: 7C (7C-I, 7C-II and 7C-III), 6C (6CE and 6C\*) and 3C (3CRR). The first thing to notice is a statistically significant difference (at the  $> 95\%$  level) between the 7C and 3C points across the whole redshift range apart from the lowest redshift bin which has a large uncertainty for the 7C sample due to few objects. We confirm the result of Eales et al. (1997), Jarvis et al. (2001a) and Inskip et al. (2002) that 6C radio galaxies are significantly fainter than 3C radio galaxies at high-redshifts, but appear to be similar at  $z < 0.6$ . Inskip et al. used a Bayesian statistical approach to show that in fact the two samples are consistent (at the 95% level) with having  $\Delta K$  between 0.1 and 0.4 magnitudes at all red-

<sup>1</sup> Jarvis et al. (2001a) used a similar dataset and the same cosmological model as in this paper and quoted the mean  $K$ -band luminosity of radio galaxies as  $5 L_*$ . This was due to their use of  $M_K^*$  from Gardner et al. (1997), although the text states that the value of  $M_K^*$  used was from the more recent derivation by Kochanek et al. (2000). This does not affect any of their other results.

shifts and so there is no strong evidence that the apparent difference between the behaviour at low and high redshifts is significant. Our analysis also confirms this and shows by the large error bars for the 6C sample at low redshifts that this uncertainty is due to the small numbers of sources. The 7C sample, which contains considerably more low-redshift sources, shows no change in the typical  $\Delta K$  at low redshifts. Therefore, attempts to describe the changing behaviour of the radio-luminosity dependence of the  $K - z$  relation at low redshifts are probably unnecessary (e.g. Best et al. 1998).

In the discussions above we have excluded the possibility that the correlation of  $\Delta K$  with radio luminosity is due to contamination of the  $K$ -band flux by non-stellar emission associated with the AGN, which would be positively correlated to the radio luminosity. Our data have been corrected for emission line contamination so this is unlikely to be the cause of the correlation. Also, Jarvis et al. (2001a) showed that the emission line contribution to the  $K$ -band magnitudes is only serious at  $z > 2$  where the strong H $\alpha$  and [OIII] lines are redshifted into the  $K$ -band. Other possible AGN-related emission mechanisms are partially obscured quasar nuclei, scattered quasar continuum and jet-induced star-formation. These issues have been investigated in detail by Leyshon & Eales (1998), Best et al. (1988), Simpson et al. (1999). Their conclusions are that the bulk of the  $K$ -band light for  $z > 1$  3CRR radio galaxies (which are the most luminous radio galaxies known) is due to emission from stars. At the highest redshifts ( $z > 3$ ) it is possible that star formation, maybe induced by the jets, could provide a dominant contribution to the  $K$ -band flux (van Breugel et al. 1998), but this is not the case for most radio galaxies at  $z < 2$  (Pentericci et al. 2001). Our finding that the difference between the  $K - z$  relations of 3C and 7C galaxies extends down to the lowest redshifts also supports the view that AGN-emission is not responsible for the difference, since at the lowest redshifts even the 3C radio galaxies have only moderately powerful nuclei.

We have shown that there is a significant difference between the  $K - z$  relations of 3C and 7C galaxies, however there is not strong evidence for systematic differences between the 6C and 7C samples in the binned data. To quantify the amount by which all the samples differ we have calculated the mean offset from the best fitting  $K - z$  relation of each sample over the redshift range  $0.2 < z < 1.8$ . This redshift range restriction is due to the paucity of 6C and 7C sources at  $z < 0.2$  and 3C sources at  $z > 1.8$ . The mean  $\Delta K$  for each sample is -0.28 for 3C, +0.05 for 6C and +0.27 for 7C. These values are indicated by the horizontal lines on Fig. 3 with the grey shading the  $\pm 1\sigma$  standard errors. They show a systematic trend of fainter  $K$ -magnitudes in lower radio luminosity galaxies.

Our finding that the 6C radio galaxies are only 0.3 mag fainter than those of 3C galaxies is much lower than the 0.6 mag difference found by Eales et al. (1997). The reason for this different result is that we have included sources at all redshifts, whereas Eales et al. (1997) separated the  $z > 0.6$  and  $z < 0.6$  galaxies and found the value of 0.6 mag for the high-redshift galaxies only. Our difference of 0.3 mag at all redshifts fits well with the analysis of Inskip et al. (2002). McCarthy (1999) showed that the  $K - z$  relation for the MRC radio galaxies (selected at a radio flux-density a factor of four lower than the 3C sample) follow essentially

the same  $K - z$  relation as the 3C sample, with MRC galaxies being only 0.2 mag systematically fainter than 3C galaxies. They claimed this is inconsistent with the 0.6 mag difference for the 3C and 6C samples from Eales et al. (1997). Apart from any biases in the MRC sample due to its spectroscopic incompleteness, it is clear that with our reduced value of the difference between the 3C and 6C samples, the MRC results are perfectly consistent.

The 0.55 mag difference in the mean  $\Delta K$  for the 3C and 7C samples, combined with the factor of 20 difference in their median 151 MHz flux-densities, implies that, on average, the stellar luminosity is higher by a factor  $\approx 1.5$  for radio galaxies which are more powerful by a factor 10.

#### 4.1 Evolution of host luminosity at constant radio luminosity

Figs. 2 and 3 have shown that within each flux-density limited sample the passive evolution description provides a good fit to the evolution of the  $K$ -magnitudes. Now we investigate the apparent cosmic evolution in host luminosities at a constant radio luminosity. This is important because the rapid decline in the space density of powerful radio sources at late cosmic epochs (e.g. Dunlop & Peacock 1990; Willott et al. 2001) means that powerful radio sources are triggered much less frequently at low redshifts. But are they triggered in the same sorts of galaxies?

To investigate this, we use the passive evolution model with  $z_f = 10$  to determine the  $K$ -magnitude of an  $L_*$  galaxy as a function of redshift. A galaxy with this evolution in  $K$ -magnitude will therefore have a constant mass with no merging and just passive evolution of the stellar population. For each galaxy in our sample, we can now calculate the evolved host luminosity in terms of a multiple of  $L_*$ . The galaxy luminosities range from 0.3 to  $14 L_*$  with a median of  $3.2 L_*$ . The few highest luminosity objects are likely to have their  $K$ -magnitudes brightened by non-stellar emission or recent star-formation, but these outliers will not strongly affect our results since only 15 of the 204 sources have luminosities  $> 6 L_*$ .

We only consider the range in redshift up to  $z = 2$  because beyond this the evolution corrections become much more uncertain (e.g. the sharp divergence of the  $z_f = 5$  and  $z_f = 10$  models in Fig. 2). In Fig. 4 we plot low-frequency radio luminosity against redshift for the radio galaxies in the complete samples up to  $z = 2$ . The galaxies are binned in radio luminosity and redshift as shown in the figure. The bins were chosen to roughly separate out the sources into their parent samples and enable the evolution in host luminosity at a constant radio luminosity to be determined. Looking at the mean evolved host luminosities shown in the figure, it is clear that the hosts tend to get relatively less luminous at higher redshifts. This occurs for all three radio luminosity slices, although the significance of the change is only  $\sim 2\sigma$  in each case. The change in host luminosity from low to high redshifts is  $\approx -1 L_*$ .

The fact that the evolved host luminosities decrease at higher redshifts can be interpreted as a change in the typical masses of the galaxies emitting a certain radio luminosity as a function of redshift. Note that because of our conservative assumption of using the  $z_f = 10$  passive evolution model, this is a lower limit to the change in mass with red-



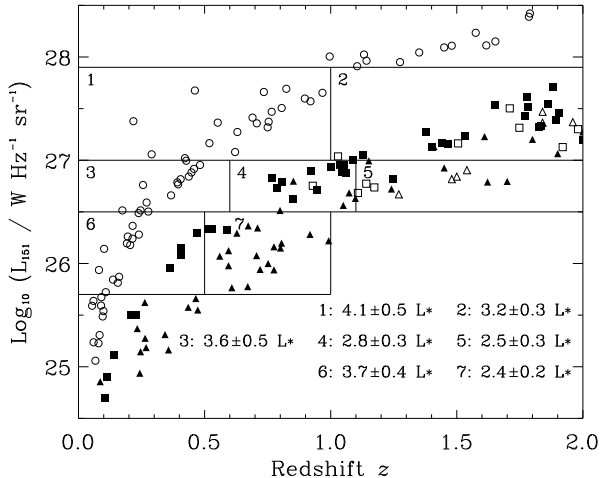


**Figure 4.** Radio luminosity at 151 MHz ( $L_{151}$ ) against redshift  $z$  for radio galaxies in the complete samples (symbols as for Fig. 2). The galaxies have been binned in terms of  $L_{151}$  and  $z$  and the mean evolved host luminosity in each bin is shown in the bottom-right corner of the plot along with its associated standard error.

shift – any later star-formation than  $z = 10$  would tend to increase the change in mass with redshift. This change in the masses of radio galaxies with redshift can be interpreted simply with the rapid evolution in the radio luminosity function from  $z = 0$  to  $z = 2$ . It is likely that the correlation between the black hole mass and stellar mass observed at low redshifts (Magorrian et al. 1998) exists to some extent at all redshifts. In this case, the typically higher radio luminosities of galaxies of a certain mass at higher redshifts may be simply the consequence of a higher average accretion rate onto a black hole of given mass, perhaps due to the greater mass of gas available to fuel the activity (e.g. Archibald et al. 2001). Other effects may be important. For example, the environmental density profiles into which jets of a given power propagate are likely to be systematically different at different redshifts. If, because of such environmental effects, sources of a given radio luminosity have lower average jet power at high  $z$  than low  $z$ , then the galaxy mass difference could again be an artifact of a weak correlation between black hole mass and jet power as discussed in Sec. 4.

Kauffmann & Haehnelt (2000) use a semi-analytic  $\Lambda$ CDM-based galaxy formation model to predict that the host galaxies of luminous ( $M_B \approx -26$ ) quasars at  $z = 2$  would be  $\approx 5$  times less massive than at  $z = 0.5$ . The radio galaxies in our highest luminosity bin have similar radio luminosities to radio-loud quasars with  $M_B \approx -26$ . We find the negative evolution in host luminosity (mass) in our bins with median redshifts  $z = 0.7$  to  $z = 1.8$  to be only a factor of 1.3. Even in a  $z_f = 3$  passive evolution model the evolution in host mass over this redshift interval would be a factor of 2.0. This is at odds with the expectations of Kauffmann & Haehnelt unless there is a significant difference in the types of galaxies hosting radio-loud and radio-quiet quasars such as a lower limit to the mass of radio-loud quasar hosts. However, the similar cosmic evolution of the two types of quasar (Willott et al. 1998) argues against such an interpretation.

Indeed, Kukula et al. (2001) compared the host luminosities of radio-quiet quasars with matched nuclear luminosities at various redshifts out to  $z = 2$  and found a similar decrease of at most a factor of two in the host luminosity.

## 5 CONCLUSIONS

We have presented  $K$ -band imaging for the 49 radio galaxies in regions 7C-I and 7C-II of the 7C Redshift Survey. This sample is selected at a low radio frequency of 151 MHz and a flux-density level a factor of 20 lower than the 3CRR sample. The 7C-I and 7C-II data have been combined with other complete samples to define the near-infrared Hubble diagram for a total of 205 radio galaxies at redshifts ranging from 0.05 to 4.4 and investigate the radio-luminosity dependence of the near-infrared magnitudes.

The  $K - z$  relation is well fit by a second order polynomial between  $K$ -magnitude and  $\log_{10} z$ :

$$K = 17.37 + 4.53 \log_{10} z - 0.31 (\log_{10} z)^2 \quad (2)$$

This curve is very close to the expected  $K$ -magnitude evolution of a passively evolving instantaneous starburst model galaxy which formed at  $z_f = 10$  with present day luminosity of  $3 L_*$ . The rms dispersion about this relation is found to be 0.58 magnitudes at all redshifts up to  $z = 3$ . These results are consistent with a high formation redshift ( $z_f > 5$ ) for radio galaxies.

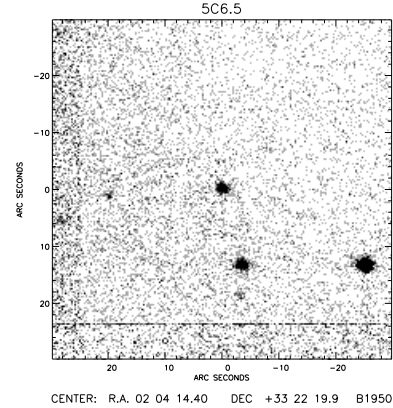
Using samples of radio galaxies selected at different flux-density limits, we have investigated the radio luminosity dependence of the  $K - z$  relation. We find that there is a significant difference between the  $K$ -magnitudes of the 3CRR and the fainter 7C radio galaxies over all redshifts. This is best interpreted as being due to a correlation of both properties with black hole mass. The typical evolution-corrected host luminosities decrease at higher redshifts by a factor in the range 1.3-2. This corresponds to a small decrease in the masses of radio galaxies at higher redshifts. The weakness of these correlations of host properties with radio luminosity and redshift aid the interpretation of the strong cosmic evolution of the radio source population. The evolution is due to a higher accretion rate in galaxies of a given mass, presumably due to an increased available mass of gas as fuel supply.

## ACKNOWLEDGEMENTS

We would like to thank Mark Lacy, Steve Eales, Gary Hill and Julia Riley for their contributions to the 7C Redshift Survey. We thank the staff at the UKIRT for their excellent technical support. The United Kingdom Infrared Telescope is operated by the Joint Astronomy Centre on behalf of the U.K. Particle Physics and Astronomy Research Council. We acknowledge the UKIRT Service Programme for some of the near-infrared imaging. CJW thanks PPARC and the National Research Council of Canada for support. MJJ acknowledges the support of the European Community Research and Training Network “The Physics of the Intergalactic Medium”. KMB thanks the Royal Society for a University Research Fellowship.

## REFERENCES

- Archibald E.N., Dunlop J.S., Hughes D.H., Rawlings S., Eales S.A., Ivison R.J., 2001, MNRAS, 323, 417
- Best P.N., Longair M.S., Röttgering H.J.A., 1998, MNRAS, 295, 549
- Bettoni D., Falomo R., Fasano G., Govoni F., Salvo M., Scarpa, R., 2001, A&A, 380, 471
- Bruzual G., Charlot S., 2002, in prep.
- Casali M., Hawarden T., 1992, JCMT-UKIRT Newsletter, No. 4, 33
- Cole S., Lacey C.G., Baugh C.M., Frenk C.S., 2000, MNRAS, 319, 168
- De Breuck C., et al. 2001, AJ, 121, 1241
- De Breuck C., van Breugel W., Stanford S.A., Röttgering H.J.A., Miley G., Stern D., 2002, AJ, 123, 637
- de Vries W.H., O'Dea C.P., Perlman E., Baum S.A., Lehnert M.D., Stocke J., Rector T., Elston R., 1998, ApJ, 503, 138
- Eales S.A., Rawlings S., 1993, ApJ, 411, 67
- Eales S.A., Rawlings S., Dickinson M., Spinrad H., Hill G.J., Lacy M., 1993, ApJ, 409, 578
- Eales S.A., Rawlings S., Law-Green J.D.B., Cotter G., Lacy M., 1997, MNRAS, 291, 593
- Ferrarese L., Merritt D., 2000, ApJ, 539, L9
- Gebhardt K., et al. 2000, ApJ, 539, L13
- Hutchings J.B., Neff S.G., 1997, AJ, 113, 550
- Inskip K.J., Best P.N., Longair M.S., MacKay D.J.C., 2002, MNRAS, 329, 277
- Irwin M.J., Maddox S.J., McMahon R.G., 1994, Spectrum: Newsletter of the Royal Observatories, 2, 14
- Jarvis M.J., Rawlings S., Eales S.A., Blundell K.M., Bunker A.J., Croft S., McLure R.J., Willott C.J., 2001a, MNRAS, 326, 1585
- Jarvis M.J., et al., 2001b, MNRAS, 326, 1563
- Kauffmann G., Haehnelt M., 2000, MNRAS, 311, 576
- Kukula M.J., Dunlop J.S., McLure R.J., Miller L., Percival W.J., Baum S.A., O'Dea C.P., 2001, MNRAS, 326, 1533
- Laing R.A., Riley J.M., Longair M.S., 1983, MNRAS, 204, 151
- Lacy M., Bunker A.J., Ridgway S.E., 2000, AJ, 120, 68
- Leyshon G., Eales, S.A., 1998, MNRAS, 295, 10
- Lilly S.J., Longair M.S., 1984, MNRAS, 211, 833
- Magorrian J., et al., 1998, AJ, 115, 2285
- McCarthy P.J., 1999, in 'The Most Distant Radio Galaxies', eds H.J.A. Röttgering, P.N. Best and M.D. Lehnert, Amsterdam, 5
- Pearson T.J., Kus A.J., 1978, MNRAS, 182, 273
- Pentericci L., McCarthy P.J., Röttgering, H.J.A., Miley G.K., van Breugel W.J.M., Fosbury R., 2001, ApJS, 135, 63
- Rawlings S., Saunders R., 1991, Nature, 349, 138
- Rawlings S., Lacy M., Leahy J.P., Dunlop J.S., Garrington S.T., Ludke E., 1996, MNRAS, 279L, 13
- Rawlings S., Eales S., Lacy M., 2001, MNRAS, 322, 523
- Simpson C., Rawlings S., Lacy M., 1999, MNRAS, 306, 828
- Simpson C., Ward M.J., Wall J.V., 2000, MNRAS, 319, 963
- Somerville R.S., Primack J.R., 1999, MNRAS, 310, 1087
- Stockton A., Canalizo G., Ridgway S.E., 1999, ApJ, 519L, 131
- van Breugel W.J.M., Stanford A.J., Spinrad H., Stern D., Graham J.R., 1998, ApJ, 502, 614
- Willott C.J., 2001, in 'AGN in their Cosmic Environment', eds B. Rocca-Volmerange & H. Sol, EDPS Conf. Series in Astron. & Astrophysics, 109
- Willott C.J., Rawlings S., Blundell K.M., Lacy M., 1998, MNRAS, 300, 625
- Willott C.J., Rawlings S., Blundell K.M., Lacy M., 1999, MNRAS, 309, 1017
- Willott C.J., Rawlings S., Blundell K.M., 2001, MNRAS, 324, 1
- Willott C.J., Rawlings S., Blundell K.M., Lacy M., Hill G.J., Scott S.E., 2002, MNRAS, 335, 1120

Figure A1.  $K$ -band image of a 7C-I quasar.

## APPENDIX A: NEAR-INFRARED IMAGES OF QUASARS IN 7C-I AND 7C-II

All members of the 7C-I and 7C-II samples have been imaged at  $K$ -band by us except the flat-spectrum quasar 5C 7.230 and the radio galaxy 3C 200. Redshifts, spectra and multi-wavelength photometry of the 24 quasars and 2 broad line radio galaxies were presented in Willott et al. (1998). In this appendix we present the  $K$ -band images for these sources so that they can be used as finding charts.

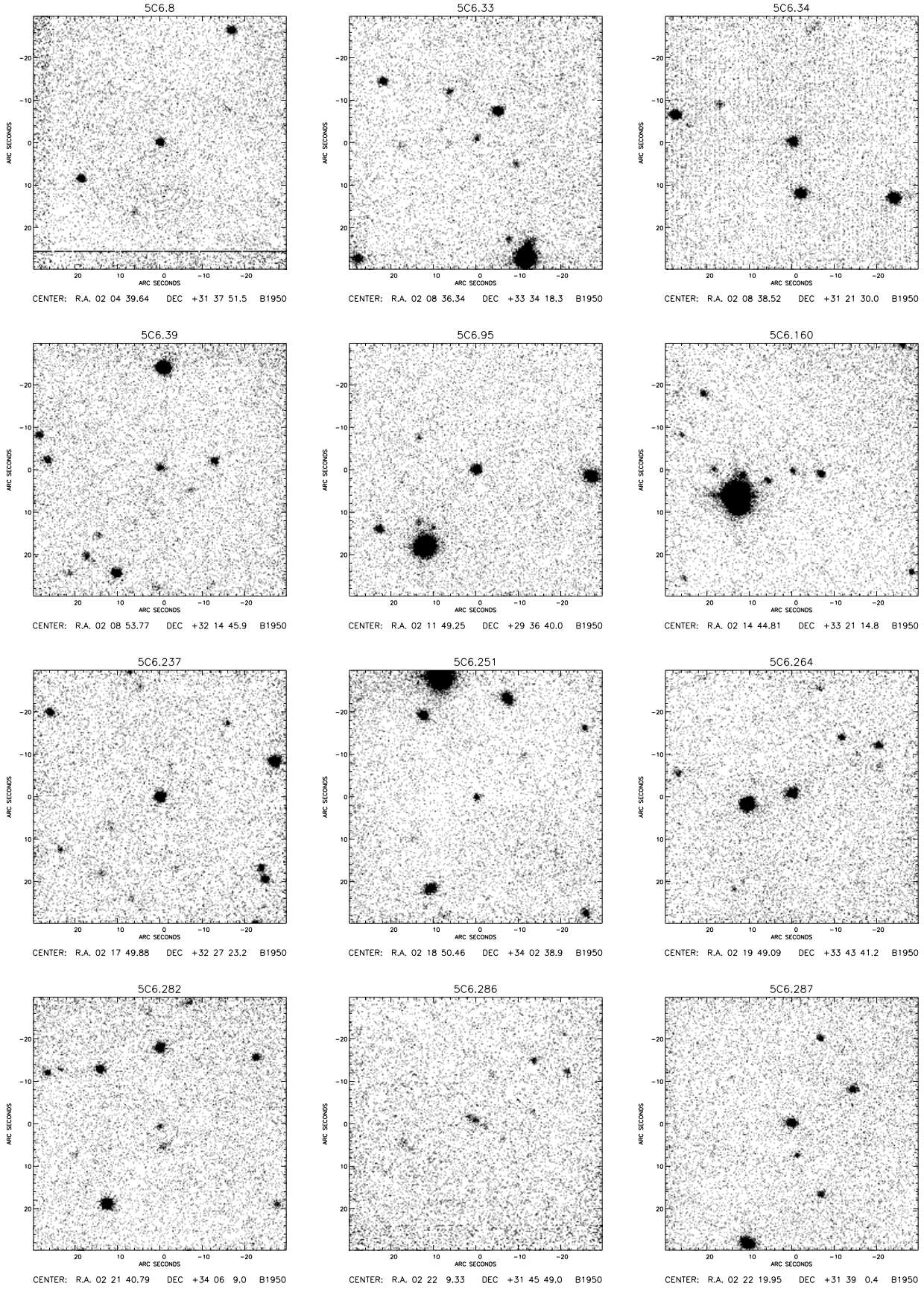


**Figure A1.** *K*-band images of 7C-I/II quasars.

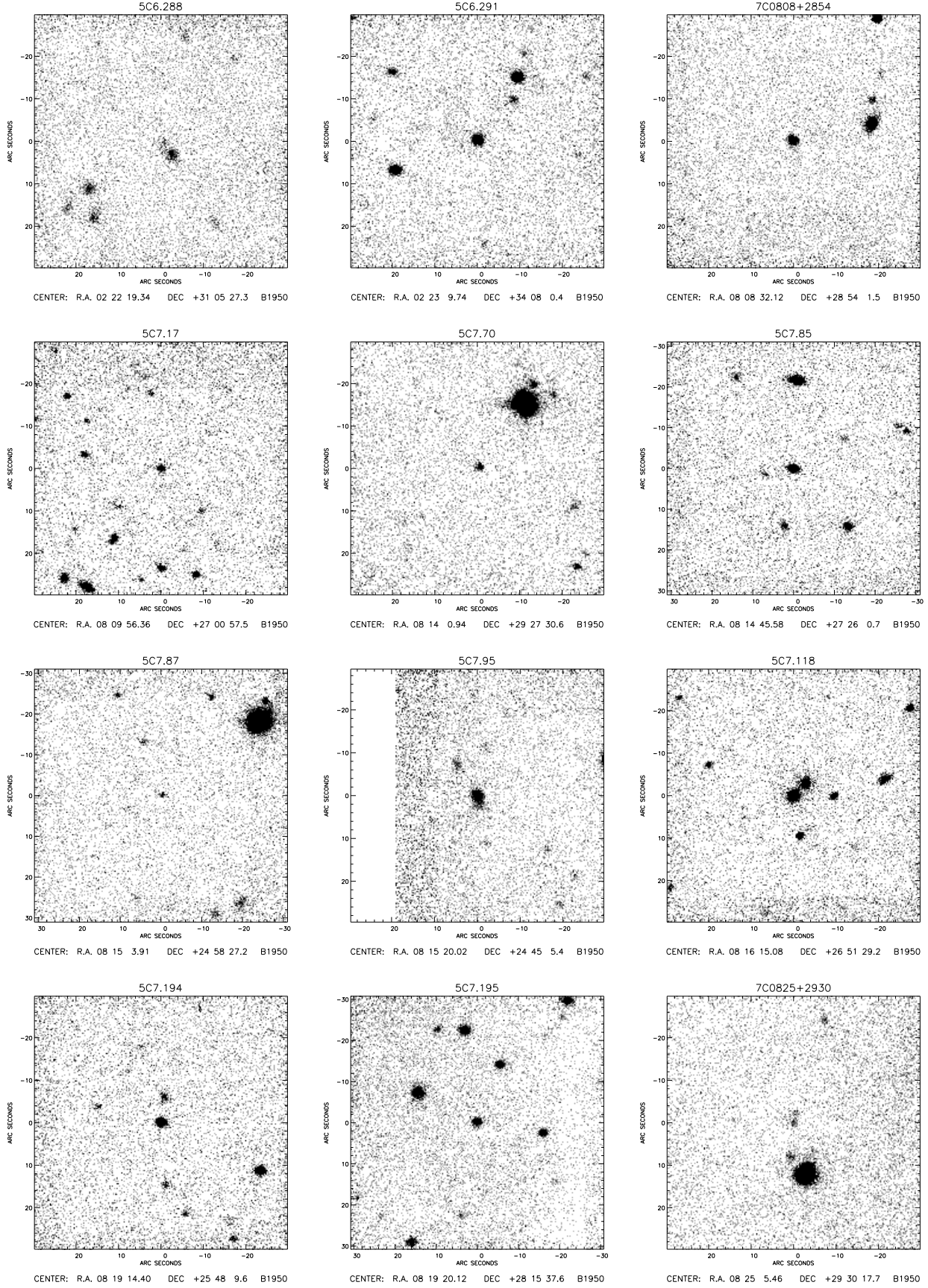


Figure A1.  $K$ -band images of 7C-I/II quasars.